

Joint probes of dark matter annihilation from neutrino detectors and CMB targets

Ruifeng Leng^a and Shao-Ping Li^b

^a*School of Physics, Sun Yat-Sen University, Guangzhou 510275, China*

^b*Marietta Blau Institute for Particle Physics, Austrian Academy of Sciences, Dominikanerbastei 16, A-1010 Vienna, Austria*

E-mail: lengrf@mail.sysu.edu.cn, Shaoping.Li@oeaw.ac.at

ABSTRACT: Dark matter (DM) annihilation into neutrinos provides a promising observational channel targeted by current and forthcoming neutrino detectors. However, the detection of such neutrino fluxes alone cannot uniquely determine their astrophysical or cosmological origin, such as the recent observations from Super-Kamiokande that hint at a small excess of electron antineutrino events. We propose that the effective number of neutrino species and the spectral distortion of the cosmic microwave background (CMB) can serve as complementary observables to probe neutrino signatures from DM annihilation. Using a simple model-independent analysis, we determine the detection windows of these cosmic observables that overlap with the experimental sensitivities from the Super-Kamiokande, Jiangmen Underground Neutrino Observatory, Hyper-Kamiokande, and the Deep Underground Neutrino Experiment, showing that joint probes of large DM annihilation to neutrinos with MeV-GeV masses can be achieved by neutrino detectors and CMB experiments.

Contents

1	Introduction	1
2	Neutrino energy release after neutrino decoupling	3
2.1	Simulation of intermediate DM production	3
2.2	Spectrum of neutrino injection	4
2.3	Modification to N_{eff}	7
3	Formation of CMB spectral distortions from neutrino annihilation	8
3.1	Photon heating from electron-positron pairs	8
3.2	The CMB μ distortion	11
4	Neutrino detectors meet the targets for the early Universe	13
5	Conclusion	16
A	Analytic derivation of injected neutrino distribution and extra radiation	17
A.1	Injected neutrino distribution f_{ν}^{inj}	17
A.2	Energy density and contribution to N_{eff}	20

1 Introduction

Dark matter (DM) annihilation into neutrinos of the standard model (SM) remains the least constrained channel in current DM indirect detection, which has created a striking platform for several neutrino detectors and telescopes to measure the neutrino fluxes in astrophysical and cosmological scales, covering a wide range of DM masses in Borexino [1, 2], KamLAND [3, 4], Jiangmen Underground Neutrino Observatory (JUNO) [5–7], Super-Kamiokande (SK) [8–12], Hyper-Kamiokande (HK) [13], Deep Underground Neutrino Experiment (DUNE) [14, 15], IceCube [16, 17], and among other things.

Remarkably, recent data release by combining the SK-gadolinium phase [18, 19] hints at a small excess of electron antineutrino events, which can reach a significant level of 2.3σ when all SK runs are combined [20–23]. Still, it is to be confirmed experimentally, and if positive, to be determined whether such an excess comes from diffuse supernova neutrino background [24–26] or new physics, especially related to the origin of neutrino masses and DM physics. When it comes to the cosmic origin, such as MeV-scale DM annihilation [27–32], it raises an important question of how we can identify such cosmic origins by using observational strategies beyond the terrestrial neutrino detectors.

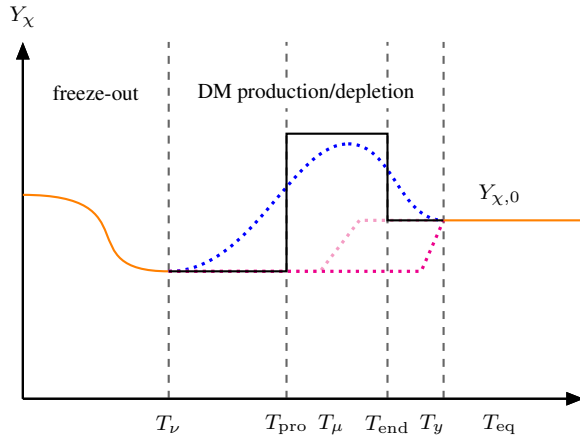


Figure 1. The density-deficit problem in DM annihilation to neutrinos, where the DM evolution with an intermediate stage of production must be present to increase the relic density from the thermal freeze-out value to the present-day value at $T_{\text{eq}} \sim 1$ eV. Freeze-out may occur as late as the neutrino decoupling temperature, $T_\nu \sim 10$ keV–1 MeV, and the intermediate state takes place at any time between T_ν and T_{eq} . The DM density yield $Y_\chi \equiv n_\chi/s$ eventually reaches its present-day value, with multiple trajectories illustrating different intermediate production histories for resolving the density-deficit problem.

For DM annihilation with mass from MeV to GeV scale, nevertheless, as pointed out in Ref. [32], most of the detection sensitivities in SK, JUNO, HK, and DUNE require a DM annihilation cross section larger than the standard thermal freeze-out value $2.2 \times 10^{-26} \lesssim \langle \sigma v \rangle / [\text{cm}^3/\text{s}] \lesssim 8 \times 10^{-26}$ [33, 34]. This implies that, for a constant DM annihilation, DM would once be in thermal equilibrium with neutrinos at the neutrino decoupling epoch, but the relic abundance from thermal freeze-out would be insufficient to account for the observed relic density today. This will introduce a *DM density-deficit problem*: for a large DM annihilation rate into neutrinos to induce observable neutrino fluxes, an intermediate stage of DM production must be present to replenish the DM abundance after thermal freeze-out. In particular, one would also be confronted by the density-deficit problem if one aims to test the SK antineutrino excess from MeV-scale DM annihilation via the upcoming JUNO and HK experiments [35, 36].

A generic illustration of the density-deficit problem is shown in Fig. 1. DM freeze-out can occur as late as the neutrino decoupling temperature, $T_\nu \sim 10$ keV–1 MeV [37–43]. After freeze-out, an intermediate stage of DM production, possibly followed by depletion, must take place to compensate for the over-annihilated DM density. This may occur during the epochs when primordial spectral distortions of the cosmic microwave background (CMB) could form, such as the μ distortion at $T_\mu \approx 0.47$ keV or the y distortion at $T_y \approx 12$ eV [44, 45]. Finally, the density yield Y_χ , defined as the DM number density over the entropy density, should reach its present-day value $Y_{\chi,0}$ at the matter-radiation equality epoch $T_{\text{eq}} \sim 1$ eV. In general, observations of neutrino fluxes in neutrino detectors alone cannot uniquely determine the intermediate DM production.

In this work, we propose the use of the effective number of neutrino species N_{eff} and the CMB μ distortion as potentially complementary observables to probe the patterns of large DM annihilation to neutrinos. We adopt a simple model-independent analysis to determine the detection

windows of N_{eff} and the CMB μ distortion, providing the parameter space for these cosmic observables that can be combined with the observations from neutrino detectors to test the neutrino signals from DM annihilation. The feasibility of such a combination is based on the following considerations. After neutrinos fully decouple at T_ν , DM annihilation to neutrinos can still generate a significant shift of N_{eff} [32], leaving impacts on recombination processes that can be detected by using the current CMB experimental techniques. On the other hand, when the cosmic temperature cools down to T_μ , secondary electromagnetic energy injection from neutrino pair annihilation or coannihilation with the relic neutrino background can perturb the photon bath [46]. At this stage, photon-number-changing processes, i.e., double Compton scattering and bremsstrahlung, become insufficient under cosmic expansion. This can lead to the formation of the primordial CMB μ distortion [44, 45], intermediate spectral distortions [47, 48] and the y distortion; see also Ref. [49]. The current bound from COBE/FIRAS gives: $|\mu| < 9 \times 10^{-5}$, $|y| < 1.5 \times 10^{-5}$ [50, 51]¹, while the forecast detection limits will be enhanced up to three orders of magnitude from future mission programs, including BISO [54], COSMO [55], TMS [56], SPECTER [57], PIXIE [58, 59], super-PIXIE [60], and Voyage 2050 [61].

The different trajectories shown in Fig. 1 may be induced by some specific particle-physics models such as the neutrinophilic DM scenarios [62–65], but we will adopt in this work a simple model-independent parametrization represented by the black line in Fig. 1 to simulate the cosmic impacts. While extra contributions to the considered cosmic observables can also appear in the specific model, such an analysis can only be conducted in a case-by-case way. Instead, our model-independent strategy allows one to focus on the effects entirely from DM annihilation to neutrinos. The resulting conclusions, therefore, should be taken as irreducible contributions for the class of DM models featuring the production history approximated by the black line. In this circumstance, we find that, for light DM at the MeV to 10 GeV scale, significant observational overlap of N_{eff} and the CMB μ distortion with the sensitivity of SK, JUNO, HK, and DUNE exists, illustrating thereby that complementary cosmic signals from DM annihilation into neutrinos beyond the terrestrial neutrino detectors are natural expectations of resolving the DM density-deficit problem.

2 Neutrino energy release after neutrino decoupling

2.1 Simulation of intermediate DM production

As shown in Fig. 1, after DM freezes out from the thermal plasma, its density yield $Y_\chi \equiv n_\chi/s$ is smaller than the current value $Y_{\chi,0}$ due to a larger annihilation cross section, where n_χ is the DM number density and

$$s = \frac{2\pi^2}{45} g_s(T) T^3, \quad (2.1)$$

denotes the SM entropy density with $g_s(T)$ the effective number of relativistic degrees of freedom. Before the Universe cools down to T_{eq} , there must be an intermediate stage to create extra DM abundances. It could occur through hidden particle decay or annihilation from superweakly-interacting massive particles [66, 67] or in first-order phase transitions [68–70]. In general, there

¹Also see Refs. [52, 53] that improved the bounds by a factor of 2.

are two kinds of evolution for the DM abundance during this intermediate stage. It may be gradually increased to accidentally match the present-day value in the end, as shown by the magenta curves in Fig. 1. Alternatively, it could first be produced overabundantly, which is then followed by depletion to match $Y_{\chi,0}$, as represented by the blue curve.

While the precise evolution of Y_χ generally requires a case-by-case treatment, one can adopt suitable approximations to capture the dominant effects. In particular, one may focus on the largest value of Y_χ obtained within a limited time interval, and identify both its typical magnitude and the corresponding period relevant for inducing observable consequences. The estimated Y_χ and the associated time interval can then be mapped onto the parameter space once a specific underlying scenario is considered. For a model-independent analysis, we adopt the following parameterization to describe an intermediate DM production:

$$Y_\chi \equiv 4.37 \times 10^{-7} \left(\frac{1 \text{ MeV}}{m_\chi} \right) [f_\chi \theta(T_{\text{pro}} - T) \theta(T - T_{\text{end}}) + 1], \quad (2.2)$$

where f_χ denotes the largest or peak abundance during a short time period $T \in [T_{\text{end}}, T_{\text{pro}}]$. The product of the two Heaviside step functions restricts the enhancement to this intermediate stage. This may correspond to the plateau of the black curve shown in Fig. 1. Here, T_{pro} denotes the temperature for the DM production reaching the maximum, and T_{end} denotes the end of Y_χ residing at the maximum.

The approximation used in Eq. (2.2) guarantees that when the production and depletion end at $T < T_{\text{end}}$, the relic yield Y_χ would match the present-day value: $\Omega_\chi h^2 \approx 0.12$ [71]. Whenever necessary, we will comment on why the parameterization of Eq. (2.2) is reasonable. By adopting Eq. (2.2), we neglect the sub-dominant contributions during the production and depletion processes that feature a smaller f_χ . We will specify the regimes in which neutrino injection in the early Universe will create observable impacts through N_{eff} and the CMB spectral distortion, and identify the regions of parameter space that overlap with the sensitivities of neutrino detectors. For this purpose, we should emphasize that Eq. (2.2) should be treated as a benchmark parameterization that can shed light on the underlying physics for the intermediate DM production. In addition, all the cosmic impacts considered below entirely come from the effects caused by DM annihilation to neutrinos. Since extra contributions to the cosmic observables may also arise in a specific particle-physics model beyond the pure DM annihilation effects, our results presented in this work should be taken as an irreducible and conservative estimate for patterns of large DM annihilation to neutrinos.

2.2 Spectrum of neutrino injection

Different from long-lived particle decays in the early Universe [46, 72–74], where dominant neutrino injection only appears at the lifetime scale of the decaying particle, DM annihilation persists even after DM has decoupled from the thermal plasma in the early Universe. Therefore, any signals from DM annihilation to neutrinos in present-day DM halos will reflect the same process in earlier epochs. This is the case if the DM annihilation rate is independent of the DM velocity. For annihilation scaling with the DM velocity, the resulting impacts are more significant at earlier times, given that the DM velocity not long after freeze-out is much larger than that at present-day typical galaxies. For these velocity-dependent annihilation to neutrinos, however, it implies that the thermally

averaged annihilation rate at freeze-out will be much larger than the present-day rate required for observations in neutrino detectors, and hence the DM density-deficit problem becomes even worse. Given this, we will focus on the case of a constant rate for DM annihilation into neutrinos, i.e., the so-called s -wave annihilation.

For DM masses in the range of a few MeV to tens GeV, upcoming experiments such as JUNO, HK, and DUNE are expected to improve the sensitivity to the annihilation cross section by about one order of magnitude compared with current bounds. For such low-scale DM masses, constraints from Big-Bang nucleosynthesis (BBN) and the CMB anisotropies are generally weaker than those derived from neutrino injection at energies above the electroweak scale [74, 75, 75]. In particular, electroweak gauge boson cascades are absent for light DM below the electroweak scale, making the associated observational effects from neutrino injection more easily tractable. For heavier DM annihilation, on the other hand, the collision rate would be suppressed by a larger neutrino energy and by a smaller DM number density, such that a significant annihilation rate would typically require larger couplings between the DM and neutrinos, which may introduce more challenges for the class of neutrinophilic DM scenarios. Note that neutrinos injected after the SM neutrino decoupling at $T \lesssim 10$ keV are hard to rethermalize with the background relic neutrinos when the injected energy is lower than 10 GeV. This can be quantified by comparing the neutrino interaction rate Γ_ν with the Hubble expansion rate H . The total neutrino cross section follows the standard Fermi-theory scaling $\sigma_\nu \sim G_F^2 s$, where s is the Mandelstam variable. For scattering with a thermal background, one has $s \sim E_\nu T$ up to an $\mathcal{O}(1)$ angular factor [76]. Here $G_F \approx 1.167 \times 10^{-5} \text{ GeV}^{-2}$ is the Fermi constant. The interaction rate can then be estimated as

$$\Gamma_\nu \sim n_\nu \langle \sigma_\nu v \rangle \sim G_F^2 E_\nu T^4, \quad (2.3)$$

where $n_\nu \sim T^3$ is the number density of background neutrinos. With the Hubble parameter in the radiation-dominated epoch,

$$H = 1.66 \sqrt{g_\rho(T)} \frac{T^2}{M_{\text{P}}}. \quad (2.4)$$

where $M_{\text{P}} = 1.22 \times 10^{19} \text{ GeV}$ is the Planck mass and $g_\rho(T)$ is the effective number of relativistic degrees of freedom in the energy density, we find that the injected neutrino energy E_ν should satisfy

$$\left(\frac{E_\nu}{10 \text{ GeV}} \right) \gtrsim \left(\frac{10 \text{ keV}}{T} \right)^2, \quad (2.5)$$

to have $\Gamma_\nu > H$. This indicates that, although neutrinos are typically decoupled at $T \sim 10$ keV, the injected neutrinos being sufficiently energetic can still undergo efficient scattering with the background neutrinos. In particular, for $E_\nu \gg 10$ GeV at $T \sim 10$ keV, the neutrino interaction rate can become comparable to or exceed the Hubble expansion rate. In this regime, scattering off the background neutrinos is no longer negligible, and the evolution of injected neutrinos is governed by the combined effects of DM annihilation, subsequent scattering processes, and cosmic expansion. In contrast, for the DM mass below 10 GeV that will be considered in this work, the injected neutrinos remain out of equilibrium, and scattering between the injected neutrinos and the

background plasma can be neglected. Under this approximation, the injected neutrino distribution can be determined by the following Boltzmann equation

$$\frac{df_\nu^{\text{inj}}}{dt} = \frac{\partial f_\nu^{\text{inj}}}{\partial t} - H|\mathbf{p}| \frac{\partial f_\nu^{\text{inj}}}{\partial |\mathbf{p}|} = \mathcal{C}_\nu, \quad (2.6)$$

where $|\mathbf{p}|$ is the neutrino momentum, and the collision term \mathcal{C}_ν accounts for neutrino production from DM annihilation $\chi\bar{\chi} \rightarrow \nu\bar{\nu}$,

$$\mathcal{C}_\nu = \frac{1}{2E_\nu} \int \left(\prod_{i=\chi, \bar{\chi}, \bar{\nu}} d\Pi_i \right) (2\pi)^4 \delta^4(p_\chi + p_{\bar{\chi}} - p_\nu - p_{\bar{\nu}}) |\mathcal{M}|^2 f_\chi f_{\bar{\chi}}, \quad (2.7)$$

with the Lorentz-invariant phase-space measure defined as²

$$d\Pi_i \equiv \frac{d^3 p_i}{(2\pi)^3} \frac{1}{2E_i}. \quad (2.8)$$

We assume homogeneous and isotropic distribution functions for both neutrinos and DM, such that $f_\nu^{\text{inj}}(t, \mathbf{x}, \mathbf{p}) = f_\nu^{\text{inj}}(t, |\mathbf{p}|)$ and $f_\chi(t, \mathbf{x}, \mathbf{p}) = f_\chi(t, |\mathbf{p}|)$, as appropriate at the background level in an expanding universe with isotropic DM annihilation. We consider symmetric DM, for which the particle and antiparticle distribution functions coincide, $f_\chi = f_{\bar{\chi}}$. The annihilation process is taken to occur after DM has become nonrelativistic, with the amplitude \mathcal{M} evaluated accordingly. The coupling of DM to the neutrino flavors is model dependent. For simplicity, we assume here that DM annihilates into the three SM neutrino flavors with approximately equal annihilation rates. In this setup, the total rate of DM annihilation into neutrinos is given by $3\mathcal{C}_\nu$, and hence the solution f_ν^{inj} denotes the single-flavor distribution of the injected neutrinos. Finally, we have taken the SM neutrinos to be Dirac fermions for definiteness, but the following conclusions are qualitatively unchanged for Majorana neutrinos.

For the s -wave nonrelativistic DM annihilation, the squared amplitude $|\mathcal{M}|^2$ has a simple relation to the thermally averaged cross section³,

$$\langle \sigma v \rangle \approx \frac{|\mathcal{M}|^2}{32\pi m_\chi^2}, \quad (2.9)$$

and the collision rate reduces to

$$\mathcal{C}_\nu = \frac{2\pi^2 \langle \sigma v \rangle}{E_\nu^2} n_\chi^2 \delta(E_\nu - m_\chi). \quad (2.10)$$

We then obtain an analytic solution by integrating along the phase-space characteristic:

$$f_\nu^{\text{inj}}(t, |\mathbf{p}|) = \int_{t_{\text{pro}}}^t dt' \mathcal{C}_\nu(t', |\mathbf{p}(t')|) = \frac{2\pi^2 \langle \sigma v \rangle}{m_\chi^3 H(t_*)} n_\chi^2(t_*) \theta(t_* - t_{\text{pro}}) \theta(t - t_*), \quad (2.11)$$

²We use $d^3 p$ to denote integration over three-momentum, which should not be confused with the four-momentum inside the Dirac- δ function.

³See Appendix A for more details.

where we impose the vanishing initial condition $f_\nu^{\text{inj}}(t_{\text{pro}}, |\mathbf{p}|) = 0$, and use the neutrino dispersion relation

$$E_\nu(t') = |\mathbf{p}| \frac{a(t)}{a(t')}, \quad \dot{E}_\nu(t') = -|\mathbf{p}| \frac{a(t)\dot{a}(t')}{a^2(t')} = -E_\nu(t')H(t'), \quad (2.12)$$

which defines the resonant time $t_*(t, E_\nu)$ through the condition $E_\nu(t_*) = m_\chi$. Introducing the dimensionless variables

$$r \equiv \frac{E_\nu}{T}, \quad x \equiv \frac{T_{\text{pro}}}{T}, \quad r_\chi \equiv \frac{m_\chi}{T_{\text{pro}}}, \quad (2.13)$$

and substituting the parameterization of the intermediate DM yield from Eq. (2.2) into Eq. (2.11), we arrive at

$$f_\nu^{\text{inj}}(x, r) = \frac{2\pi^2 M_{\text{P}}^* \langle \sigma v \rangle T_{\text{pro}}^2}{m_\chi r^4} \Theta^2 \theta(r - r_\chi) \theta(r_\chi x - r), \quad (2.14)$$

where $M_{\text{P}}^* \approx 0.45 M_{\text{P}} / \sqrt{g_\rho(T_*)}$. In general, the effective relativistic degrees of freedom for entropy and energy densities differ, $g_s(T) \neq g_\rho(T)$. However, after neutrino decoupling, we can adopt $g_s(T) \approx g_\rho(T) \approx 3.34$, which is a good approximation for the temperature range of interest [77]. The two Heaviside step functions in Eq. (2.14) have distinct physical origins. $\theta(r - r_\chi)$ arises from the redshift of the neutrino energy from the production epoch T_{pro} to the observation temperature T , while $\theta(r_\chi x - r)$ encodes the kinematic upper bound associated with nonrelativistic DM annihilation. Given the parameterization of Eq. (2.2), an additional Heaviside step function is effectively encoded in the function Θ , which originates from the time (or equivalently temperature) dependence of the DM number density n_χ :

$$\Theta \equiv 10^{-4} \left(\frac{10 \text{ keV}}{T_{\text{pro}}} \right) [f_\chi \theta(r - r_\chi) \theta(T_{\text{pro}} r_\chi - T_{\text{end}} r) + 1]. \quad (2.15)$$

Note that the overall scaling of f_ν^{inj} is independent of the T_{pro} choice, since the explicit dependence cancels in the product $T_{\text{pro}}^2 \Theta^2$.

2.3 Modification to N_{eff}

The neutrino abundance generated by DM annihilation after neutrino decoupling contributes to the radiation energy density and can therefore modify N_{eff} :

$$N_{\text{eff}}^{\text{inj}} = \frac{8}{7} \left(\frac{11}{4} \right)^{4/3} \left(\frac{2\rho_\nu^{\text{inj}}}{\rho_\gamma} \right), \quad (2.16)$$

where $2\rho_\nu^{\text{inj}}$ denotes the energy density carried by the injected neutrinos and antineutrinos from DM annihilation, and

$$\rho_\gamma = \frac{\pi^2}{15} T^4, \quad (2.17)$$

is the background photon energy density. Here, $N_{\text{eff}}^{\text{inj}}$ should be understood as the shift of the standard N_{eff} caused by extra radiation energy density. ρ_ν^{inj} can be computed from the single-flavor injected distribution f_ν^{inj} , i.e., from Eq. (2.14), via

$$\rho_\nu^{\text{inj}} = \sum_{\alpha=e,\mu,\tau} \int \frac{d^3p}{(2\pi)^3} E_\nu f_{\nu\alpha}^{\text{inj}} \approx 3 \int \frac{d^3p}{(2\pi)^3} E_\nu f_\nu^{\text{inj}}, \quad (2.18)$$

where the last approximation is derived by the consideration that the DM annihilation rates into three neutrino flavors share the similar order. Unless there is a strong hierarchy among the DM-neutrino flavor couplings, the above result works to a good approximation, owing to the fast redistribution through neutrino oscillations. From Eq. (2.18), we arrive at

$$N_{\text{eff}}^{\text{inj}}(T) \approx 0.0056 \left(\frac{\langle\sigma v\rangle}{10^{-24} \text{ cm}^3/\text{s}} \right) \left(\frac{1 \text{ MeV}}{m_\chi} \right) (\mathcal{F}_{\text{int}} + \mathcal{F}_{\text{rel}}), \quad (2.19)$$

where \mathcal{F}_{int} accounts for the contribution from intermediate DM production

$$\mathcal{F}_{\text{int}} \equiv f_\chi(f_\chi + 2)\theta(T_{\text{pro}} - T) \left[\theta(T - T_{\text{end}}) \ln \left(\frac{T_{\text{pro}}}{T} \right) + \theta(T_{\text{end}} - T) \ln \left(\frac{T_{\text{pro}}}{T_{\text{end}}} \right) \right], \quad (2.20)$$

while \mathcal{F}_{rel} represents the contribution from relic DM annihilation in the absence of intermediate production⁴

$$\mathcal{F}_{\text{rel}} \equiv \theta(T_{\text{pro}} - T) \ln \left(\frac{T_{\text{pro}}}{T} \right). \quad (2.21)$$

To compare with cosmological observations, we evaluate the above expression at the epoch of photon decoupling, $T = T_{\text{CMB}} \approx 0.26 \text{ eV}$, which sets the radiation content probed by CMB anisotropies. This yields

$$N_{\text{eff}}^{\text{inj}} \approx 0.0056 \left(\frac{\langle\sigma v\rangle}{10^{-24} \text{ cm}^3/\text{s}} \right) \left(\frac{1 \text{ MeV}}{m_\chi} \right) \left[f_\chi(f_\chi + 2) \ln \left(\frac{T_{\text{pro}}}{T_{\text{end}}} \right) + \ln \left(\frac{T_{\text{pro}}}{T_{\text{CMB}}} \right) \right]. \quad (2.22)$$

Note that varying T_{pro} , T_{end} , T_{CMB} by an order of magnitude typically induces only a subleading change in $N_{\text{eff}}^{\text{inj}}$ at the level of $\mathcal{O}(0.1)\%$.

3 Formation of CMB spectral distortions from neutrino annihilation

3.1 Photon heating from electron-positron pairs

The injected neutrino energy will subsequently be converted into light SM particles once kinematic thresholds are open. Given the fact that the number density of injected neutrinos is generally much smaller than that of background thermal relic neutrinos, it has previously been anticipated that pair annihilation of injected neutrinos has a suppressed rate, compared with the coannihilation between background neutrinos and injected neutrinos [78–80]. However, studies on the disintegration of

⁴The contribution from \mathcal{F}_{rel} is consistent with Ref. [32] after accounting for a total of three neutrino flavors. The small numerical difference derived here is caused by using a more precise DM relic density adopted in Eq. (2.2).

light elements formed at BBN have shown that pair annihilation of ultrahigh-energy neutrinos can also make a non-negligible contribution to secondary electromagnetic cascades [74, 81, 82], owing to the larger center-of-mass energy. We also note that, after e^+e^- annihilation, scattering of injected neutrinos off background electrons is strongly suppressed, since charge neutrality implies $n_e \simeq n_b$, making the relic electron density much smaller than the photon density by the baryon-to-photon ratio $n_e/n_\gamma \simeq \eta_b \sim 10^{-10}$.

For electron-positron pair production through coannihilation $\nu_{\text{inj}} + \bar{\nu}_{\text{bg}} \rightarrow e^- + e^+$, the injected neutrino energy must satisfy the approximate kinematic threshold

$$E_\nu^{\text{inj}} \gtrsim \frac{m_e^2}{T_\nu^{\text{bg}}}, \quad (3.1)$$

where $T_\nu^{\text{bg}} \sim T$ is the temperature of the background relic neutrinos, and we have estimated the typical background neutrino energy as $E_\nu^{\text{bg}} \sim T$. In particular, for CMB spectral distortions generated as early as $T_\mu = 0.47$ keV [44, 45], a DM mass larger than roughly 500 MeV is required for coannihilation to proceed efficiently. If most neutrino injections occur at $T > T_\mu$, the neutrino energy would redshift to a smaller value at T_μ , such that the DM mass should be larger to open the coannihilation channel at T_μ for generating potential CMB spectral distortions. By contrast, for pair annihilation among injected neutrinos, $\nu_{\text{inj}} + \bar{\nu}_{\text{inj}} \rightarrow e^- + e^+$, the threshold for converting the injected neutrino energy into an electron-positron pair is much lower,

$$E_\nu^{\text{inj}} \gtrsim m_e. \quad (3.2)$$

This is because both incoming neutrinos are energetic, unlike in the coannihilation channel where the background relic neutrino is soft.

For MeV-scale DM annihilating into neutrinos, electromagnetic energy transfer can already proceed through pair annihilation of the injected neutrinos. By contrast, coannihilation in this regime is subject to a strong Boltzmann suppression at T_μ , with a factor $\sim e^{-m_e/T_\mu}$ from the high-energy tail of the thermal relic-neutrino distribution. In the following, we consider both pair annihilation and coannihilation channels for electron-positron pair production. We neglect final-state radiation processes that directly produce photons, such as $\nu + \bar{\nu} \rightarrow e^- + e^+ + \gamma$, since they are higher order in the electromagnetic coupling. Although such processes can receive logarithmic enhancements in the infrared regime, the contribution of soft photons to CMB spectral distortions before recombination is expected to be small [83]. The produced electron-positron pairs will rapidly lose energy through repeated inverse Compton scattering with background photons, $e^\pm + \gamma_{\text{bg}} \rightarrow e^\pm + \gamma$, thereby heating the background photons. If the electron-positron pairs are relativistic, only a small fraction of the injected neutrino energy is stored in the electron and positron rest masses. The dominant energy-loss channel is then inverse Compton scattering with background photons [84–86], whose rate is much larger than the Hubble expansion rate before recombination. The heated photons subsequently redistribute their energy through Compton scattering with the residual background electrons, $\gamma + e_{\text{bg}}^- \rightarrow \gamma + e^-$, producing CMB spectral distortions as early as $T = T_\mu$.

In general, the energy-transfer rate into electron-positron pairs can be written as

$$\frac{d\rho_{e\bar{e}}}{dt} = \sum_{\alpha=e,\mu,\tau} \int \left(\prod_{i=\nu_\alpha, \bar{\nu}_\alpha, e, \bar{e}} d\Pi_i \right) (E_e + E_{\bar{e}}) (2\pi)^4 \delta^4(p) |\mathcal{M}_{\nu_\alpha \bar{\nu}_\alpha \rightarrow e\bar{e}}|^2 f_{\nu_\alpha} f_{\bar{\nu}_\alpha}, \quad (3.3)$$

where $d\Pi_i$ is defined in Eq. (2.8), and $\delta^4(p) \equiv \delta^4(p_{\nu_\alpha} + p_{\bar{\nu}_\alpha} - p_e - p_{\bar{e}})$. We take the summation of the energy-transfer rate over three neutrino flavors, and have neglected the Pauli-blocking effect for the final-state electron-positron pairs. For the coannihilation channel, we will take $f_{\nu_\alpha} f_{\bar{\nu}_\alpha} = f_{\nu_\alpha}^{\text{inj}} f_{\bar{\nu}_\alpha}^{\text{bg}}$ for definiteness, and then multiply the resulting rate by a factor of two to include the charge-conjugate process $\bar{\nu}_{\text{inj}} + \nu_{\text{bg}} \rightarrow e^- + e^+$. For pair annihilation, both the neutrino distribution functions in Eq. (3.3) are given by Eq. (2.14). It is worth mentioning again that for temperatures below ~ 10 keV, neutrino oscillations are much faster than the Hubble expansion [87, 88], and the oscillation time is also much shorter than the relevant scattering time. Therefore, neutrinos injected by DM annihilation in a given flavor state will instantaneously redistribute among the three flavors. For DM annihilation to three neutrino flavors considered in this work, it is then a good approximation to use Eq. (2.14) for each neutrino flavor that participates in the electron-positron pair production.

Using energy conservation, $E_e + E_{\bar{e}} = E_{\nu_\alpha} + E_{\bar{\nu}_\alpha}$, we first perform the final-state electron-positron phase-space integration in the center-of-mass frame, yielding

$$\int d\Pi_e d\Pi_{\bar{e}} (2\pi)^4 \delta^4(p_{\nu_\alpha} + p_{\bar{\nu}_\alpha} - p_e - p_{\bar{e}}) |\mathcal{M}_{\nu_\alpha \bar{\nu}_\alpha \rightarrow e\bar{e}}|^2 = \frac{G_F^2 s^2}{3\pi} \mathcal{G}_\alpha \theta(s - 4m_e^2), \quad (3.4)$$

where G_F denotes the Fermi constant, $s = (p_{\nu_\alpha} + p_{\bar{\nu}_\alpha})^2$ is the Mandelstam variable, and $\theta(s - 4m_e^2)$ is the Heaviside step function enforcing the electron-positron production threshold. The flavor-dependent function \mathcal{G}_α is given by

$$\mathcal{G}_\alpha = \left(1 + \frac{2m_e^2}{s} \right) g_W^\alpha - \frac{3m_e^2}{s}, \quad (3.5)$$

where

$$g_W^e = (1 + 4 \sin^2 \theta_W + 8 \sin^4 \theta_W), \quad g_W^\mu = g_W^\tau = (1 - 4 \sin^2 \theta_W + 8 \sin^4 \theta_W), \quad (3.6)$$

with θ_W being the weak mixing angle and $\sin^2 \theta_W \approx 0.22$. In the present estimate, we include the flavor dependence through the coupling factor \mathcal{G}_α . The $\nu_e + \bar{\nu}_e \rightarrow e^- + e^+$ channel gives the leading contribution, since it receives both charged-current and neutral-current contributions, while the $\nu_\mu \bar{\nu}_\mu$ and $\nu_\tau \bar{\nu}_\tau$ channels proceed only through neutral-current interactions and are suppressed relative to the $\nu_e \bar{\nu}_e$ channel by $g_W^{\mu,\tau} / g_W^e \simeq 0.22$.

Next, it becomes straightforward to complete the calculation of the energy-transfer rate by applying the neutrino distribution functions. For the coannihilation channel, the relic neutrino background is described by the Fermi-Dirac distribution

$$f_\nu^{\text{bg}}(E_\nu) = \frac{1}{e^{E_\nu/T_\nu^{\text{bg}}} + 1}, \quad (3.7)$$

and we neglect the small difference between the three flavors. Furthermore, we take, for simplicity, the neutrino temperature to be the one following the standard neutrino decoupling $T_\nu^{\text{bg}} = (4/11)^{1/3}T$. While the modification of N_{eff} in general induces a shift of this temperature ratio, the impact is small when evaluating the energy-transfer rate. For pair annihilation, on the other hand, both of the two neutrino distribution functions are given by Eq. (2.14). Because the integrand contains several kinematic step functions, we will evaluate Eq. (3.3) numerically.

3.2 The CMB μ distortion

In this section, we will consider the formation of the CMB μ distortion, which can be accurately described by using semi-analytic methods. The extension to the formation of the y distortion and intermediate-type distortions [47, 48] can also be taken, but requires full numerical solutions of the spectral-distortion equations. Nevertheless, we should mention that, since both of the intermediate-type distortions and the y distortion are formed at a later stage, intermediate DM production at these later epochs could lead to stronger impacts at the matter-radiation equality and recombination epochs, suffering more severe constraints from large-scale structure formation and CMB anisotropies. For intermediate DM production at much earlier times, on the other hand, the generation of these intermediate-type and y distortions would require heavier DM since the redshift effect of the injected neutrino energy is stronger.

The heating rate of the background photons induced by the kinetic energy of the electron-positron pairs can then be approximated as

$$\frac{d\rho_\gamma}{dt} \approx \frac{d\rho_{e\bar{e}}}{dt}. \quad (3.8)$$

Although not all of the energy stored in the electron-positron pairs is converted into photon energy, Eq. (3.8) provides a good approximation for predicting the resulting μ distortion for relativistic e^\pm [84–86, 89]. After the subsequent Comptonization, the transferred photon energy generates a primordial μ distortion in the background photon distribution during the epoch $12 \text{ eV} \lesssim T \lesssim 0.47 \text{ keV}$, corresponding to the redshift $z_y \equiv 5 \times 10^4 \lesssim z \lesssim 2 \times 10^6 \equiv z_\mu$ [44, 45, 49], which will survive to the present day. The well established analytic formula yields [89–91]

$$\mu \approx 1.4 \int_0^\infty \mathcal{J}_\mu(z) \frac{1}{\rho_\gamma} \frac{d\rho_\gamma}{dt} \left| \frac{dt}{dz} \right| dz, \quad (3.9)$$

where μ denotes the dimensionless chemical-potential parameter characterizing the CMB spectral distortion. ρ_γ in the denominator is the unperturbed blackbody photon energy density, which serves as the normalization for the injected energy. $d\rho_\gamma/dt$ is the rate of the electromagnetic energy-injection into the photon bath. We use $|dt/dz| \approx 7.3 \times 10^{37}/(1+z)^3 \text{ keV}^{-1}$, and $\mathcal{J}_\mu(z)$ is the visibility function for the epoch during which the μ distortion is formed [92, 93]

$$\mathcal{J}_\mu(z) = e^{-(z/z_\mu)^{5/2}} \theta(z - z_y). \quad (3.10)$$

The exponential factor above accounts for the erasure of distortions at sufficiently high redshift, where photon-number-changing processes efficiently restore a blackbody spectrum, while the step function restricts the formation epoch to the μ -distortion era.

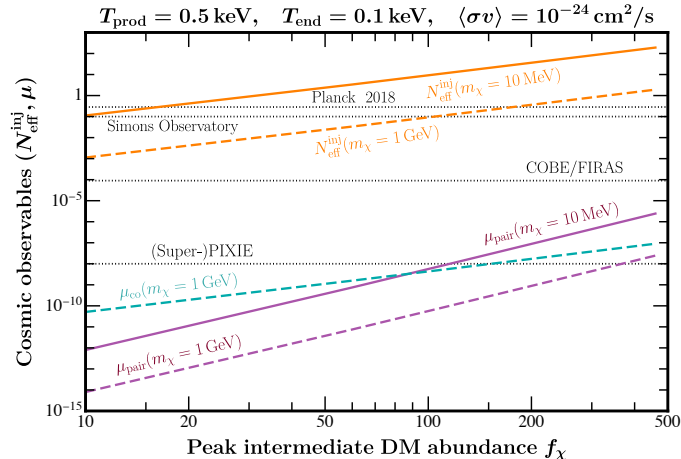


Figure 2. Modification of N_{eff} , denoted by $N_{\text{eff}}^{\text{inj}}$, and the CMB μ distortion as functions of the peak intermediate DM abundance f_χ . The coannihilation and pair annihilation contributions to the μ distortion are denoted by μ_{co} and μ_{pair} , respectively. Injected neutrinos arise from DM annihilation during $T \in [0.1, 0.5]$ keV, with a reference annihilation cross section near the projected sensitivities of JUNO [5, 6, 30], HK [13, 94, 95], and DUNE [30, 96]. For comparison, we show the COBE/FIRAS bound $|\mu| < 9 \times 10^{-5}$ [50, 51], a representative future sensitivity $|\mu| \simeq 10^{-8}$ for (Super-)PIXIE [59], the Planck limit $N_{\text{eff}}^{\text{inj}} \lesssim 0.285$ [71], and the projected Simons Observatory sensitivity $N_{\text{eff}}^{\text{inj}} \simeq 0.1$ [97, 98].

The integration in Eq. (3.9) can be done numerically by substituting the energy-deposition rate obtained in Eq. (3.3). In Fig. 2, we show the resulting $N_{\text{eff}}^{\text{inj}}$ together with the μ distortion induced by coannihilation, μ_{co} , and by pair annihilation, μ_{pair} . We fix the annihilation cross section to be $\langle\sigma v\rangle = 10^{-24} \text{ cm}^3/\text{s}$, which is of the typical order targeted by upcoming neutrino detectors such as JUNO [5, 6, 30], HK [13, 94, 95], and DUNE [30, 96]; see also Ref. [30]. We take the intermediate DM production to occur over the relatively short temperature interval $T \in [0.1, 0.5]$ keV. Enlarging the interval over which the peak abundance f_χ is maintained does not significantly modify the predictions for either $N_{\text{eff}}^{\text{inj}}$ or the μ distortion.

The reason for the rather weak sensitivity of both $N_{\text{eff}}^{\text{inj}}$ and the μ distortion on the intermediate interval temperature can be understood as follows. During the period in which f_χ is active, $N_{\text{eff}}^{\text{inj}}$ depends only logarithmically on the duration of the production epoch, $N_{\text{eff}}^{\text{inj}} \propto \ln(T_{\text{pro}}/T_{\text{end}})$, as can be inferred from Eq. (2.20). Therefore, increasing the range of temperatures over which the intermediate abundance persists only leads to a mild change in $N_{\text{eff}}^{\text{inj}}$. By contrast, for pair annihilation, the integrand in Eq. (3.9) scales approximately as T . This follows from the scaling of the injected neutrino distribution $f_\nu^{\text{inj}} \propto T^4$, given in Eq. (2.14), together with $1/\rho_\gamma \propto T^{-4}$ and $|dt/dz| \propto T^{-3}$. For coannihilation with the neutrino background, the relic neutrino distribution is Boltzmann suppressed at low temperatures, $f_\nu^{\text{bg}} \propto e^{-1/T}$. This exponential suppression strongly reduces the coannihilation contribution to the integrand in Eq. (3.9) at late times. As a result, the contribution to the μ distortion is mainly controlled by energy deposition near the high-temperature end of the μ -distortion era, around T_μ . Extending the intermediate DM production period to lower temperatures adds only a subdominant contribution to the integral, and hence has little impact on the predicted μ distortion.

Conversely, if the intermediate DM production period is made very short, the effects on both

observables are suppressed by the small available temperature interval. For $N_{\text{eff}}^{\text{inj}}$, the logarithmic factor $\ln(T_{\text{pro}}/T_{\text{end}})$ becomes small when T_{pro} and T_{end} are close. For the μ distortion, the integrated energy deposition in Eq. (3.9) is likewise reduced because the integration range over which the source is active is narrow. Thus, in this limiting case, the impacts of intermediate production on both $N_{\text{eff}}^{\text{inj}}$ and the μ distortion are correspondingly suppressed. Nevertheless, for typical intermediate DM production, we expect that the peak abundance would not sharply evolve to vanishingly small values. These observations in turn justify the proper parameterization of the intermediate DM production via the black line shown in Fig. 1 or equivalently via Eq. (2.2).

Two representative mass choices, $m_\chi = 10$ MeV and $m_\chi = 1$ GeV, are shown in Fig. 2. For the lower mass case, the coannihilation contribution to the μ distortion is strongly suppressed. As discussed in Section 3.1, this suppression originates from the exponential feature of the high-energy thermal tail of the background neutrino distribution required to satisfy the kinematic threshold. For $m_\chi = 1$ GeV, this suppression is alleviated, and the coannihilation contribution becomes much larger. In this case, μ_{co} even exceeds μ_{pair} , indicating that coannihilation dominates the generation of the μ distortion for larger DM masses. However, this comparison can change if the peak intermediate DM abundance f_χ is increased. Since $\mu_{\text{pair}} \propto f_\chi^4$, whereas $\mu_{\text{co}} \propto f_\chi^2$, the pair annihilation contribution grows more rapidly with f_χ and can dominate for sufficiently large f_χ . A similar situation will occur for neutrino injection from relic particle decay, where pair annihilation among the neutrinos produced by the decays can become more important than coannihilation if the abundance of the relic particles at decay is sufficiently large [46].

Nevertheless, Fig. 2 allows us to draw a general conclusion that μ_{pair} cannot reach the forecast μ -distortion sensitivity without violating the N_{eff} constraint. For both benchmark masses, $m_\chi = 10$ MeV and $m_\chi = 1$ GeV, we see clearly that $N_{\text{eff}}^{\text{inj}}$ reaches the current Planck bound when μ_{pair} is still too small to reach the detection limit. In contrast, the coannihilation contribution μ_{co} can reach the detection limit while $N_{\text{eff}}^{\text{inj}}$ coincidentally reaches the projected sensitivity of future probes, e.g., Simons Observatory [97, 98], provided that the DM mass is above 500 MeV.

4 Neutrino detectors meet the targets for the early Universe

The modification of N_{eff} and the generation of the CMB μ distortion with $\langle\sigma v\rangle = 10^{-24}$ cm³/s suggest that joint CMB measurements and neutrino detectors can probe overlapping regions of parameter space with large rates of DM annihilation into neutrinos. To illustrate this point, we show in Fig. 3 the detection windows in the $(m_\chi, \langle\sigma v\rangle)$ plane, adopting the benchmark values $f_\chi = 100$, $T_{\text{pro}} = 0.5$ keV, and $T_{\text{end}} = 0.1$ keV. The left panel corresponds to the low-mass regime ($m_\chi < 100$ MeV), while the right panel shows the high-mass regime ($m_\chi > 100$ MeV). The experiment-labeled curves correspond to target values of the cosmic observables: $N_{\text{eff}}^{\text{inj}} \simeq 0.285, 0.1$ for Planck 2018 and Simons Observatory, respectively, and $|\mu| \simeq 10^{-8}, 10^{-9}$ for (Super-)PIXIE and Voyage 2050.

In the left panel of Fig. 3, the region between the Planck 2018 and Simons Observatory curves defines the target window $N_{\text{eff}}^{\text{inj}} \in [0.1, 0.285]$, which overlaps appreciably with the parameter space accessible to JUNO and HK for $m_\chi \in [10, 100]$ MeV. By contrast, the projected CMB μ -distortion sensitivities, $|\mu| \in [10^{-8}, 10^{-9}]$, require much larger annihilation cross sections in this mass range.

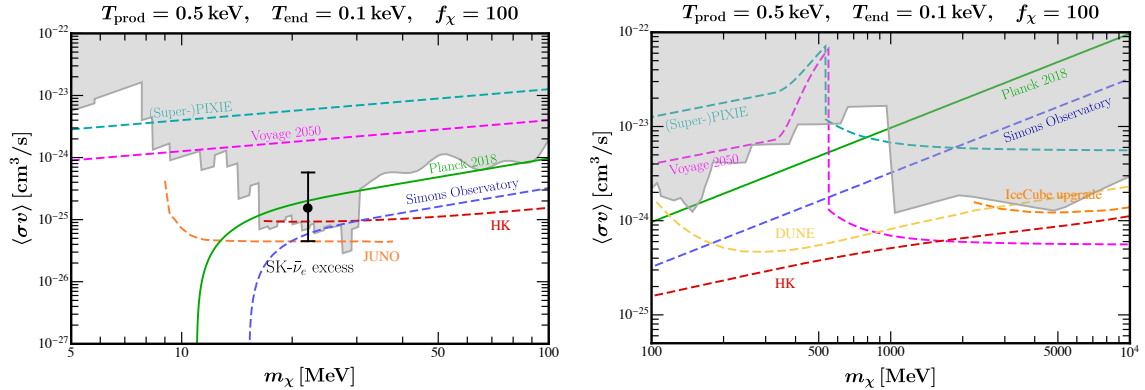


Figure 3. Detection windows for $N_{\text{eff}}^{\text{inj}}$, the CMB μ distortion, and neutrino-detector searches in the $(m_\chi, \langle\sigma v\rangle)$ plane, where $\langle\sigma v\rangle$ is the total DM annihilation cross section into all three SM neutrino flavors [30]. The cosmological curves are labeled by the corresponding limits or sensitivities: Planck 2018 for $N_{\text{eff}}^{\text{inj}} \simeq 0.285$, Simons Observatory for $N_{\text{eff}}^{\text{inj}} \simeq 0.1$, (Super-)PIXIE for $|\mu| \simeq 10^{-8}$, and Voyage 2050 for $|\mu| \simeq 10^{-9}$. Dashed curves denote future sensitivities, while solid curves and shaded regions denote current limits. Current neutrino-detector exclusions at 90% C.L. limits are from Borexino [1, 2], KamLAND [4], and SK [8–11, 99]. In the left panel, the black dot marks the SK- $\bar{\nu}_e$ best-fit point for the antineutrino excess, and the black error bar shows the corresponding 2σ region [35].

They are therefore well separated from both the $N_{\text{eff}}^{\text{inj}}$ target window and the JUNO/HK sensitivities, indicating that the CMB μ distortion is not expected to be observable in the MeV-scale region. We show the current SK- $\bar{\nu}_e$ exclusion region for $9 \text{ MeV} \lesssim m_\chi \lesssim 30 \text{ MeV}$, which is evaluated at 90% C.L. for the normalized Galactic J -factor $\mathcal{J}_{\text{avg}} = 4$ [30, 35]. The updated SK- $\bar{\nu}_e$ data by combining all the SK runs, especially including the SK-gadolinium phase, prefer a best-fit point for the antineutrino excess at $m_\chi = 22.1 \text{ MeV}$, with the black error bar indicating the corresponding 2σ range $\mathcal{J}_{\text{avg}}\langle\sigma v\rangle \in [1.8 \times 10^{-25}, 2.3 \times 10^{-24}] \text{ cm}^3/\text{s}$ [35]. We should mention here that a small portion of the 2σ SK- $\bar{\nu}_e$ excess region still remains below the current exclusion bound.

The SK- $\bar{\nu}_e$ constraint requires more accurate treatment for the astrophysical uncertainties, since it is important to confirm and test the potential SK- $\bar{\nu}_e$ excess in the MeV-mass regime, and to determine the extent to which the $N_{\text{eff}}^{\text{inj}}$ target window will overlap with the future reach of JUNO and HK. Note that the explanation of the SK- $\bar{\nu}_e$ excess does not necessarily lead to the DM density-deficit problem if one adopts the 2σ level of the observed events, as can be seen from the left panel of Fig. 3. The corresponding annihilation cross section can reach down to $\langle\sigma v\rangle \approx 5 \times 10^{-26} \text{ cm}^3/\text{s}$, comparable with the thermally averaged one predicted by the standard freeze-out. Nevertheless, this value matches the projected sensitivity of JUNO marginally and lies below that of HK. Therefore, the full confirmation and test of the SK- $\bar{\nu}_e$ excess through both JUNO and HK would introduce the density-deficit problem.

We arrive at the conclusion that a possible SK- $\bar{\nu}_e$ excess, future neutrino-detector signals, and a measurable shift in N_{eff} can probe a common region of MeV-scale DM annihilation into neutrinos. Note that the DM masses below 10 MeV are also constrained by BBN and CMB observations through their impact on neutrino decoupling [27–29, 31, 40, 42, 100–102]. However, the latest data releases from DESI [103, 104], SPT-3G [105], and ACT [106] leave the lower mass bound inconclusive [32]. Moreover, depending on the origin of the intermediate DM production, a significant

contribution to N_{eff} can arise even for $m_\chi > 10$ MeV, where it may dominate over the modification of neutrino decoupling. Therefore, a signal of $N_{\text{eff}}^{\text{inj}}$ can be correlated with extra neutrino fluxes observable at SK, JUNO, and HK for $m_\chi \in [10, 100]$ MeV.

In the right panel of Fig. 3, we show the detection windows for the higher DM mass range $m_\chi \in [100, 10^4]$ MeV. The target region between the Planck 2018 and Simons Observatory curves overlaps with the parameter space accessible to HK and DUNE. Moreover, for $m_\chi \gtrsim 500$ MeV, the region between the (super-)PIXIE and Voyage 2050 curves also enters the HK/DUNE reach, indicating that the same parameter space can be jointly probed by an observable μ distortion and $N_{\text{eff}}^{\text{inj}}$. For $m_\chi \gtrsim 1$ GeV, we notice that the predicted μ distortion depends only weakly on the DM mass, while the corresponding $N_{\text{eff}}^{\text{inj}}$ lies below 0.1. Indeed, for $m_\chi \gtrsim 500$ MeV, we can verify that the coannihilation rate in Eq. (3.3) becomes nearly independent of the DM mass. It implies that, for heavier DM, the CMB μ distortion can become the dominant cosmological probe of large annihilation rates, where substantial overlap with the regions accessible to HK and DUNE exists. This behavior is qualitatively consistent with the fact that CMB spectral distortions can be more sensitive than N_{eff} to ultrahigh-energy neutrino injection from superheavy DM or long-lived particle decay [79].

We should mention that $|\mu| \in [10^{-8}, 10^{-9}]$ opens a larger window for $m_\chi \gtrsim 500$ MeV than for $m_\chi \in [100, 500]$ MeV. This follows from the different scaling behaviors of the dominant energy-injection channels. For $m_\chi \in [100, 500]$ MeV, the CMB μ distortion is mainly induced by pair annihilation of injected neutrinos, whose rate scales approximately as $\langle\sigma v\rangle^2$. Thus, improving the μ sensitivity by one order of magnitude lowers the required cross section by roughly $\sqrt{0.1}$. For $m_\chi \gtrsim 500$ MeV, coannihilation with the relic neutrino background becomes dominant, the rate of which scales approximately linearly with $\langle\sigma v\rangle$. The same sensitivity improvement of the μ distortion then lowers the required cross section by about 0.1, producing the larger window between the (Super-)PIXIE and Voyage 2050 curves in the high-mass region.

It should also be mentioned that the kinetic threshold $m_\chi \gtrsim 500$ MeV follows from Eq. (3.1) for the benchmark choice $T_{\text{pro}} = 0.5$ keV. If both T_{pro} and T_{end} are higher than T_μ , the redshift of the injected neutrino energy becomes important, and the kinetic threshold for coannihilation shifts to larger DM masses. In the limit $T_{\text{pro}}, T_{\text{end}} \gg T_\nu \sim 1$ MeV, injected neutrinos rapidly thermalize with the background plasma, so they can no longer be treated as a late-time contribution to N_{eff} and do not form CMB spectral distortions.

As a final remark, we emphasize that the constant DM annihilation considered in this work corresponds to a DM-velocity independent annihilation cross section. The overlap between the cosmological detection windows and the neutrino-detector sensitivities found in this work depends sensitively on the intermediate DM abundance, parameterized by f_χ . Since f_χ encodes the production history, it can be used to probe the underlying particle-physics model. A joint measurement or exclusion by CMB observables and neutrino detectors would probe not only the large rates of DM annihilation into neutrinos, but also the mechanism responsible for generating and maintaining the intermediate DM abundance. We also note that the DM density-deficit problem may be relaxed in velocity-dependent annihilation. Generally, we may parameterize the thermally averaged annihilation cross section in the partial-wave method, where $\langle\sigma v\rangle = a + bv^2 + \mathcal{O}(v^4)$, and a, b correspond, respectively, to the s - and p -wave components. Then, the constant DM annihilation to neutrinos

essentially indicates $a \gg b$. When $|a| \sim |b|$ with $b < 0$, however, there may exist certain cancellation between the s - and p -wave contributions, such that the annihilation cross section at freeze-out with $v = \mathcal{O}(0.1)$ could be smaller than that at the present day with $v = \mathcal{O}(10^{-4})$. Nevertheless, a difference at orders of magnitude for $\langle\sigma v\rangle$ between the freeze-out and present-day epochs, which is needed for observations from upcoming neutrino detectors, requires a delicate fine-tuning between a and b . One such tuning may arise in the resonant production regime. In this case, DM annihilation to neutrinos occurs through an s -channel process, and the DM mass should be confined to nearly half of the mediator mass.

5 Conclusion

If DM dominantly annihilates into the SM neutrinos, it can partly explain the current null results of indirect DM detection and evade the more severe constraints from electromagnetic or hadronic energy injection in astrophysics and cosmology. Nevertheless, the weak interactions of SM neutrinos also present challenges for indirectly detecting this less constrained channel. Strikingly, several neutrino detectors, such as SK, JUNO, HK, and DUNE, will be able to detect extra neutrino fluxes potentially from DM annihilation, especially given the current hint of the SK antineutrino excess. To detect and confirm the neutrino signals, however, it would introduce the DM density-deficit problem: there must be some intermediate DM production processes to compensate for the over-annihilated DM density at freeze-out.

In this work, we have investigated the consequences of resolving the density-deficit problem by combining the detection sensitivities from terrestrial neutrino detectors with the cosmic probe from CMB experiments. Instead of building the specific particle-physics models where DM can dominantly annihilate into neutrinos, we adopt a simple strategy, which is model independent and a rather sensible parameterization, to simulate the cosmic impacts from large rates of MeV-GeV DM annihilation into neutrinos. We demonstrate that there exists a large detection overlap between neutrino detectors and CMB experiments targeting the early Universe, including the probes of the CMB μ distortion and N_{eff} . The results presented in this work are conservative in the sense that the cosmic impacts are entirely from DM annihilation to neutrinos, the same quantity that is probed by neutrino detectors. In specific particle-physics models, on the other hand, we do not exclude any possibility that may contribute additionally to the cosmic observables under consideration. In this situation, looking for DM annihilation to neutrinos complementarily through neutrino detectors and cosmic probes proposed in this work will be strengthened.

Acknowledgements

We would like to thank John Beacom for discussions at the early stage of this project. We also thank Yushi Mura for discussions on the potential UV framework for the DM density-deficit problem, and Alessandro Granelli, Silvia Pascoli, and Salvador Rosauero-Alcaraz for explanations of the SK antineutrino excess.

A Analytic derivation of injected neutrino distribution and extra radiation

In this appendix, we provide the explicit derivation of the analytic results used in Sections 2.2 and 2.3. We begin by deriving the distribution function f_ν^{inj} for neutrinos injected by DM annihilation after neutrino decoupling. We then compute the radiation energy density induced by this nonthermal component and use it to obtain the associated contribution to the effective number of neutrino species, $N_{\text{eff}}^{\text{inj}}$.

A.1 Injected neutrino distribution f_ν^{inj}

We first derive the collision term \mathcal{C}_ν that appears in the Boltzmann equation (2.6). For neutrino production from DM annihilation, $\chi\bar{\chi} \rightarrow \nu\bar{\nu}$, the collision term is constructed directly as

$$\mathcal{C}_\nu = \frac{1}{2E_\nu} \int \left(\prod_{i=\chi, \bar{\chi}, \bar{\nu}} d\Pi_i \right) (2\pi)^4 \delta^4(p_\chi + p_{\bar{\chi}} - p_\nu - p_{\bar{\nu}}) |\mathcal{M}|^2 f_\chi f_{\bar{\chi}}. \quad (\text{A.1})$$

After performing the integration over the momentum space, we obtain

$$\begin{aligned} \mathcal{C}_\nu &= \frac{1}{2E_\nu} \left(\int \frac{d^3 p_\chi}{(2\pi)^3} f_\chi \right) \left(\int \frac{d^3 p_{\bar{\chi}}}{(2\pi)^3} f_{\bar{\chi}} \right) \frac{\pi}{4E_{\bar{\nu}} E_\chi E_{\bar{\chi}}} \delta(E_\chi + E_{\bar{\chi}} - E_\nu - E_{\bar{\nu}}) |\mathcal{M}|^2 \\ &\approx \frac{\pi |\mathcal{M}|^2}{16E_{\bar{\nu}}^2 m_\chi^2} \delta(E_\nu - m_\chi) n_\chi^2, \end{aligned} \quad (\text{A.2})$$

where we take the approximation of nonrelativistic DM such that the squared amplitude $|\mathcal{M}|^2$ is both temperature and momentum independent, and the DM distribution functions can be integrated out to the number density, giving n_χ^2 for symmetric DM $n_\chi = n_{\bar{\chi}}$. In the nonrelativistic limit, $E_\chi = E_{\bar{\chi}} \simeq m_\chi$ is used, while the energy conservation condition $E_\nu = E_{\bar{\nu}} \approx m_\chi$ is time dependent due to cosmic expansion.

For the s -wave nonrelativistic DM annihilation, there is a simple relation between the squared amplitude $|\mathcal{M}|^2$ and the thermally averaged cross section $\langle\sigma v\rangle$, the latter of which is defined through the Boltzmann collision rate of the injected neutrino number density

$$\langle\sigma v\rangle n_\chi^2 \equiv \int \left(\prod_{i=\chi, \bar{\chi}, \nu, \bar{\nu}} d\Pi_i \right) (2\pi)^4 \delta^4(p_\chi + p_{\bar{\chi}} - p_\nu - p_{\bar{\nu}}) |\mathcal{M}|^2 f_\chi f_{\bar{\chi}}. \quad (\text{A.3})$$

Using a constant $|\mathcal{M}|^2$, the above integration over the phase space can be performed independently of $|\mathcal{M}|^2$, such that

$$\langle\sigma v\rangle \approx \frac{|\mathcal{M}|^2}{32\pi m_\chi^2}. \quad (\text{A.4})$$

The collision term \mathcal{C}_ν given in Eq. (A.2) can then be expressed in terms of $\langle\sigma v\rangle$

$$\mathcal{C}_\nu = \frac{2\pi^2 \langle\sigma v\rangle}{E_\nu^2} n_\chi^2 \delta(E_\nu - m_\chi). \quad (\text{A.5})$$

We now solve the Boltzmann equation for the injected neutrino distribution function

$$\frac{df_\nu^{\text{inj}}}{dt} = \frac{\partial f_\nu^{\text{inj}}}{\partial t} - H|\mathbf{p}| \frac{\partial f_\nu^{\text{inj}}}{\partial |\mathbf{p}|} = \mathcal{C}_\nu. \quad (\text{A.6})$$

The Liouville total derivative is taken along the phase-space trajectory of a freely propagating neutrino. In an expanding universe, the physical momentum redshifts as

$$\frac{d|\mathbf{p}|}{dt} = -H|\mathbf{p}|, \quad (\text{A.7})$$

or equivalently, the comoving momentum $|\mathbf{q}| \equiv a|\mathbf{p}|$ is conserved. Therefore, the dispersion relation of the injected neutrino reads

$$E_\nu(t') = |\mathbf{p}| \frac{a(t)}{a(t')}, \quad \dot{E}_\nu(t') = -|\mathbf{p}| \frac{a(t)\dot{a}(t')}{a^2(t')} = -E_\nu(t')H(t'). \quad (\text{A.8})$$

Imposing the initial condition $f_\nu^{\text{inj}}(t_{\text{pro}}, |\mathbf{p}|) = 0$, the solution is obtained by integrating the collision term along the phase-space characteristic:

$$\begin{aligned} f_\nu^{\text{inj}}(t, |\mathbf{p}|) &= \int_{t_{\text{pro}}}^t dt' \mathcal{C}_\nu(t', |\mathbf{p}|(t')) \\ &= \int_{t_{\text{pro}}}^t dt' \frac{2\pi^2 \langle \sigma v \rangle}{E_\nu^2(t')} n_\chi^2(t') \delta(E_\nu(t') - m_\chi) \\ &= \frac{2\pi^2 \langle \sigma v \rangle}{E_\nu^2(t_*)} n_\chi^2(t_*) \left| \dot{E}_\nu(t_*) \right|^{-1} \theta(t_* - t_{\text{pro}}) \theta(t - t_*) \\ &= \frac{2\pi^2 \langle \sigma v \rangle}{m_\chi^3 H(t_*)} n_\chi^2(t_*) \theta(t_* - t_{\text{pro}}) \theta(t - t_*), \end{aligned} \quad (\text{A.9})$$

where t_* is defined by

$$E_\nu(t_*) = m_\chi. \quad (\text{A.10})$$

The factor $|\dot{E}_\nu(t_*)|^{-1}$ is the Jacobian obtained when the energy δ -function is converted into a time-dependent one. The two Heaviside step functions enforce that t_* lies inside the integration range $t_{\text{pro}} < t_* < t$.

To make the redshift dependence explicit, it is convenient to trade the dimensional variables for dimensionless combinations. Since both the neutrino energy and the cosmic temperature scale approximately as a^{-1} during the epoch of interest, we therefore introduce the dimensionless variables

$$r \equiv \frac{E_\nu}{T}, \quad x \equiv \frac{T_{\text{pro}}}{T}, \quad r_\chi \equiv \frac{m_\chi}{T_{\text{pro}}}. \quad (\text{A.11})$$

The resonant condition $E_\nu(t_*) = m_\chi$ then fixes the corresponding temperature as

$$T_* = \frac{m_\chi}{r}. \quad (\text{A.12})$$

The two Heaviside functions appearing in the solution can be rewritten in terms of these dimensionless variables as

$$\begin{aligned} \theta(r - r_\chi) &= \theta\left(\frac{E_\nu}{T} - \frac{m_\chi}{T_{\text{pro}}}\right) = \theta\left(E_\nu - \frac{T}{T_{\text{pro}}}m_\chi\right) \\ &= \theta(E_\nu(t_{\text{pro}}) - m_\chi) = \theta(E_\nu(t_{\text{pro}}) - E_\nu(t_*)) = \theta(t_* - t_{\text{pro}}), \end{aligned} \quad (\text{A.13})$$

$$\begin{aligned} \theta(r_\chi x - r) &= \theta\left(\frac{m_\chi}{T} - \frac{E_\nu}{T}\right) = \theta(m_\chi - E_\nu(t)) \\ &= \theta(E_\nu(t_*) - E_\nu(t)) = \theta(t - t_*). \end{aligned} \quad (\text{A.14})$$

These relations show that the condition $t_{\text{pro}} < t_* < t$ is equivalent to the finite support

$$r_\chi \leq r \leq r_\chi x. \quad (\text{A.15})$$

Using

$$H(T_*) = 1.66\sqrt{g_\rho(T_*)}\frac{T_*^2}{M_{\text{P}}}, \quad n_\chi(T_*) = s(T_*)Y_\chi(T_*), \quad s(T_*) = \frac{2\pi^2}{45}g_s(T_*)T_*^3, \quad (\text{A.16})$$

the injected neutrino distribution function becomes

$$\begin{aligned} f_\nu^{\text{inj}}(t, |\mathbf{p}|) &= \frac{2\pi^2\langle\sigma v\rangle}{m_\chi^3 H(T_*)} s^2(T_*) Y_\chi^2(T_*) \theta(r - r_\chi) \theta(r_\chi x - r) \\ &= \left(\frac{2\pi^2}{45}\right)^2 \frac{2\pi^2 M_{\text{P}} \langle\sigma v\rangle}{m_\chi^3 1.66\sqrt{g_\rho(T_*)}} g_s^2(T_*) \left(\frac{m_\chi}{r}\right)^4 \theta(r - r_\chi) \theta(r_\chi x - r) \\ &\quad \times \left(4.37 \times 10^{-7} \left(\frac{1 \text{ MeV}}{m_\chi}\right) [f_\chi \theta(T_{\text{pro}} - T_*) \theta(T_* - T_{\text{end}}) + 1]\right)^2 \\ &= \left(\frac{2\pi^2}{45}\right)^2 \frac{g_s^2(T_*)}{1.66\sqrt{g_\rho(T_*)}} \frac{2\pi^2 M_{\text{P}} \langle\sigma v\rangle T_{\text{pro}}^5 r_\chi^3}{m_\chi^4 r^4} \theta(r - r_\chi) \theta(r_\chi x - r) \\ &\quad \times \left(4.37 \times 10^{-7} \left(\frac{1 \text{ MeV}}{10 \text{ keV}} \frac{10 \text{ keV}}{T_{\text{pro}}}\right) [f_\chi \theta(r - r_\chi) \theta(T_{\text{pro}} r_\chi - T_{\text{end}} r) + 1]\right)^2 \\ &= \frac{2\pi^2 M_{\text{P}}^* \langle\sigma v\rangle T_{\text{pro}}^2}{m_\chi r^4} \Theta^2 \theta(r - r_\chi) \theta(r_\chi x - r), \end{aligned} \quad (\text{A.17})$$

where we have defined notations

$$M_{\text{P}}^* \equiv 0.437^2 \left(\frac{2\pi^2}{45} \right)^2 \frac{g_s^2(T_*)}{1.66\sqrt{g_\rho(T_*)}} M_{\text{P}} \approx \frac{0.45}{g_\rho(T_*)} M_{\text{P}} \approx 0.246 M_{\text{P}}, \quad (\text{A.18})$$

$$\Theta \equiv 10^{-4} \left(\frac{10 \text{ keV}}{T_{\text{pro}}} \right) [f_\chi \theta(r - r_\chi) \theta(T_{\text{pro}} r_\chi - T_{\text{end}} r) + 1]. \quad (\text{A.19})$$

After neutrino decoupling, we can take $g_s(T) \approx g_\rho(T) \approx 3.34$, which is a good approximation over the temperature range considered here. The factor Θ encodes the time dependence of the DM abundance: the term proportional to f_χ selects annihilation during the intermediate production stage, while the constant term corresponds to annihilation from the final relic abundance.

A.2 Energy density and contribution to N_{eff}

We next compute the energy density carried by the injected neutrinos. This step connects the nonthermal neutrino spectrum derived above to the cosmological observable N_{eff} . Since these neutrinos are produced after neutrino decoupling and remain free streaming, their energy density behaves as an additional radiation component.

Assuming comparable rates of DM annihilation into the three SM neutrino flavors, the energy density stored in the injected neutrinos is

$$\begin{aligned} \rho_\nu^{\text{inj}} &= 3 \int \frac{d^3p}{(2\pi)^3} E_\nu f_\nu^{\text{inj}} \quad (\text{A.20}) \\ &= 3 \int \frac{|\mathbf{p}|^2 d|\mathbf{p}| d\Omega}{(2\pi)^3} E_\nu f_\nu^{\text{inj}} \\ &= 3 M_{\text{P}}^* \langle \sigma v \rangle m_\chi T^4 \times 10^{-12} \left(\frac{1 \text{ MeV}}{m_\chi} \right)^2 \\ &\quad \times \int dE_\nu \frac{1}{E_\nu} \left[f_\chi (f_\chi + 2) \theta \left(\frac{T}{T_{\text{end}}} m_\chi - E_\nu \right) + 1 \right] \theta \left(E_\nu - \frac{T}{T_{\text{pro}}} m_\chi \right) \theta (m_\chi - E_\nu). \end{aligned}$$

The remaining integral can be calculated straightforwardly to yield $\mathcal{F}_{\text{int}} + \mathcal{F}_{\text{rel}}$, where we have separated the result into the intermediate-production contribution and the relic contribution:

$$\mathcal{F}_{\text{int}} \equiv \theta(T_{\text{pro}} - T) f_\chi (f_\chi + 2) \left[\theta(T - T_{\text{end}}) \ln \left(\frac{T_{\text{pro}}}{T} \right) + \theta(T_{\text{end}} - T) \ln \left(\frac{T_{\text{pro}}}{T_{\text{end}}} \right) \right], \quad (\text{A.21})$$

$$\mathcal{F}_{\text{rel}} \equiv \theta(T_{\text{pro}} - T) \ln \left(\frac{T_{\text{pro}}}{T} \right). \quad (\text{A.22})$$

The injected neutrino energy density is therefore

$$\rho_\nu^{\text{inj}} = 3 M_{\text{P}}^* \langle \sigma v \rangle m_\chi T^4 \times 10^{-12} \left(\frac{1 \text{ MeV}}{m_\chi} \right)^2 (\mathcal{F}_{\text{int}} + \mathcal{F}_{\text{rel}}). \quad (\text{A.23})$$

We next convert this energy density into the corresponding contribution $N_{\text{eff}}^{\text{inj}}$ with the photon en-

ergy density

$$\rho_\gamma = \frac{\pi^2}{15} T^4. \quad (\text{A.24})$$

Since ρ_ν^{inj} denotes the injected neutrino contribution summed over three flavors, the corresponding antineutrinos give an additional factor of 2. Thus,

$$\begin{aligned} N_{\text{eff}}^{\text{inj}} &= 2 \times \frac{8}{7} \left(\frac{11}{4} \right)^{4/3} \left(\frac{\rho_\nu^{\text{inj}}}{\rho_\gamma} \right) \\ &= 6 \times \frac{8}{7} \left(\frac{11}{4} \right)^{4/3} \frac{1.5 \times 10^{-11}}{\pi^2} M_{\text{P}}^* \langle \sigma v \rangle (1 \text{ MeV}) \left(\frac{1 \text{ MeV}}{m_\chi} \right) (\mathcal{F}_{\text{int}} + \mathcal{F}_{\text{rel}}). \end{aligned} \quad (\text{A.25})$$

Using $M_{\text{P}}^* \simeq 0.246 M_{\text{P}}$, one finds

$$N_{\text{eff}}^{\text{inj}} \simeq 0.0056 \left(\frac{\langle \sigma v \rangle}{10^{-24} \text{ cm}^3/\text{s}} \right) \left(\frac{1 \text{ MeV}}{m_\chi} \right) (\mathcal{F}_{\text{int}} + \mathcal{F}_{\text{rel}}). \quad (\text{A.26})$$

At the CMB epoch, $T = T_{\text{CMB}}$, and for $T_{\text{CMB}} < T_{\text{end}} < T_{\text{pro}}$, this becomes

$$N_{\text{eff}}^{\text{inj}} \simeq 0.0056 \left(\frac{\langle \sigma v \rangle}{10^{-24} \text{ cm}^3/\text{s}} \right) \left(\frac{1 \text{ MeV}}{m_\chi} \right) \left[f_\chi (f_\chi + 2) \ln \left(\frac{T_{\text{pro}}}{T_{\text{end}}} \right) + \ln \left(\frac{T_{\text{pro}}}{T_{\text{CMB}}} \right) \right]. \quad (\text{A.27})$$

The first logarithm measures the duration of the intermediate stage, while the second logarithm is the relic contribution accumulated from T_{pro} to the CMB epoch. This logarithmic dependence explains why moderate variations of T_{pro} and T_{end} only mildly affect $N_{\text{eff}}^{\text{inj}}$. The full result shows how the intermediate DM production required to resolve the density-deficit problem can enhance $N_{\text{eff}}^{\text{inj}}$ and thereby provide a complementary cosmological probe of the same annihilation process. In the absence of intermediate DM production, we take $\mathcal{F}_{\text{int}} = 0$, such that the expression reduces to

$$N_{\text{eff}}^{\text{inj}} = 0.0056 \left(\frac{\langle \sigma v \rangle}{10^{-24} \text{ cm}^3/\text{s}} \right) \left(\frac{1 \text{ MeV}}{m_\chi} \right) \ln \left(\frac{T_{\text{pro}}}{T_{\text{CMB}}} \right), \quad (\text{A.28})$$

recovering the irreducible neutrino injection from the final relic abundance [32].

References

- [1] **Borexino** Collaboration, G. Bellini et al., *Study of solar and other unknown anti-neutrino fluxes with Borexino at LNGS*, *Phys. Lett. B* **696** (2011) 191–196, [[arXiv:1010.0029](#)].
- [2] **Borexino** Collaboration, M. Agostini et al., *Search for low-energy neutrinos from astrophysical sources with Borexino*, *Astropart. Phys.* **125** (2021) 102509, [[arXiv:1909.02422](#)].
- [3] **KamLAND** Collaboration, A. Gando et al., *A study of extraterrestrial antineutrino sources with the KamLAND detector*, *Astrophys. J.* **745** (2012) 193, [[arXiv:1105.3516](#)].
- [4] **KamLAND** Collaboration, S. Abe et al., *Limits on Astrophysical Antineutrinos with the KamLAND Experiment*, *Astrophys. J.* **925** (2022), no. 1 14, [[arXiv:2108.08527](#)].

- [5] **JUNO** Collaboration, F. An et al., *Neutrino Physics with JUNO*, *J. Phys. G* **43** (2016), no. 3 030401, [[arXiv:1507.05613](#)].
- [6] K. Akita, G. Lambiase, M. Niibo, and M. Yamaguchi, *Neutrino lines from MeV dark matter annihilation and decay in JUNO*, *JCAP* **10** (2022) 097, [[arXiv:2206.06755](#)].
- [7] **JUNO** Collaboration, A. Abusleme et al., *JUNO sensitivity to the annihilation of MeV dark matter in the galactic halo*, *JCAP* **09** (2023) 001, [[arXiv:2306.09567](#)].
- [8] **Super-Kamiokande** Collaboration, J. Hosaka et al., *Solar neutrino measurements in super-Kamiokande-I*, *Phys. Rev. D* **73** (2006) 112001, [[hep-ex/0508053](#)].
- [9] **Super-Kamiokande** Collaboration, J. P. Cravens et al., *Solar neutrino measurements in Super-Kamiokande-II*, *Phys. Rev. D* **78** (2008) 032002, [[arXiv:0803.4312](#)].
- [10] **Super-Kamiokande** Collaboration, K. Abe et al., *Solar neutrino results in Super-Kamiokande-III*, *Phys. Rev. D* **83** (2011) 052010, [[arXiv:1010.0118](#)].
- [11] **Super-Kamiokande** Collaboration, K. Bays et al., *Supernova Relic Neutrino Search at Super-Kamiokande*, *Phys. Rev. D* **85** (2012) 052007, [[arXiv:1111.5031](#)].
- [12] A. Olivares-Del Campo, C. Boehm, S. Palomares-Ruiz, and S. Pascoli, *Dark matter-neutrino interactions through the lens of their cosmological implications*, *Phys. Rev. D* **97** (2018), no. 7 075039, [[arXiv:1711.05283](#)].
- [13] **Hyper-Kamiokande** Collaboration, K. Abe et al., *Hyper-Kamiokande Design Report*, [[arXiv:1805.04163](#)].
- [14] **DUNE** Collaboration, R. Acciarri et al., *Long-Baseline Neutrino Facility (LBNF) and Deep Underground Neutrino Experiment (DUNE): Conceptual Design Report, Volume 2: The Physics Program for DUNE at LBNF*, [[arXiv:1512.06148](#)].
- [15] F. Capozzi, S. W. Li, G. Zhu, and J. F. Beacom, *DUNE as the Next-Generation Solar Neutrino Experiment*, *Phys. Rev. Lett.* **123** (2019), no. 13 131803, [[arXiv:1808.08232](#)].
- [16] **IceCube** Collaboration, M. G. Aartsen et al., *The IceCube Neutrino Observatory: Instrumentation and Online Systems*, *JINST* **12** (2017), no. 03 P03012, [[arXiv:1612.05093](#)]. [Erratum: *JINST* **19**, E05001 (2024)].
- [17] **IceCube** Collaboration, R. Abbasi et al., *The IceCube high-energy starting event sample: Description and flux characterization with 7.5 years of data*, *Phys. Rev. D* **104** (2021) 022002, [[arXiv:2011.03545](#)].
- [18] **Super-Kamiokande** Collaboration, K. Abe et al., *First gadolinium loading to Super-Kamiokande*, *Nucl. Instrum. Meth. A* **1027** (2022) 166248, [[arXiv:2109.00360](#)].
- [19] **Super-Kamiokande** Collaboration, K. Abe et al., *Second gadolinium loading to Super-Kamiokande*, *Nucl. Instrum. Meth. A* **1065** (2024) 169480, [[arXiv:2403.07796](#)].
- [20] M. Harada, *Review of diffuse sn neutrino background*, June, 2024.
- [21] A. Santos, M. Harada, and Y. Kanemura, *New limits on the low-energy astrophysical electron antineutrinos at sk-gd experiment*, June, 2024.
- [22] R. Rogly, *Overview of the model-dependent approach for the diffuse supernova neutrino background search with the sk-gd experiment*, June, 2024.
- [23] A. Beauchêne, *Diffuse supernova neutrino background: Insights from super-kamiokande & prospects with hyper- kamiokande*, June, 2024.

- [24] K. Kotake, K. Sato, and K. Takahashi, *Explosion mechanism, neutrino burst, and gravitational wave in core-collapse supernovae*, *Rept. Prog. Phys.* **69** (2006) 971–1144, [[astro-ph/0509456](#)].
- [25] A. Mirizzi, I. Tamborra, H.-T. Janka, N. Saviano, K. Scholberg, R. Bollig, L. Hudepohl, and S. Chakraborty, *Supernova Neutrinos: Production, Oscillations and Detection*, *Riv. Nuovo Cim.* **39** (2016), no. 1-2 1–112, [[arXiv:1508.00785](#)].
- [26] S. Horiuchi and J. P. Kneller, *What can be learned from a future supernova neutrino detection?*, *J. Phys. G* **45** (2018), no. 4 043002, [[arXiv:1709.01515](#)].
- [27] S. Palomares-Ruiz and S. Pascoli, *Testing MeV dark matter with neutrino detectors*, *Phys. Rev. D* **77** (2008) 025025, [[arXiv:0710.5420](#)].
- [28] C. M. Ho and R. J. Scherrer, *Limits on MeV Dark Matter from the Effective Number of Neutrinos*, *Phys. Rev. D* **87** (2013), no. 2 023505, [[arXiv:1208.4347](#)].
- [29] C. Boehm, M. J. Dolan, and C. McCabe, *A Lower Bound on the Mass of Cold Thermal Dark Matter from Planck*, *JCAP* **08** (2013) 041, [[arXiv:1303.6270](#)].
- [30] C. A. Argüelles, A. Diaz, A. Kheirandish, A. Olivares-Del-Campo, I. Safa, and A. C. Vincent, *Dark matter annihilation to neutrinos*, *Rev. Mod. Phys.* **93** (2021), no. 3 035007, [[arXiv:1912.09486](#)].
- [31] N. Sabti, J. Alvey, M. Escudero, M. Fairbairn, and D. Blas, *Refined Bounds on MeV-scale Thermal Dark Sectors from BBN and the CMB*, *JCAP* **01** (2020) 004, [[arXiv:1910.01649](#)].
- [32] S. Kanemura, S.-P. Li, and D. Nanda, *Bounds and detection of MeV-scale dark matter annihilation to neutrinos*, *Phys. Rev. D* **112** (2025), no. 3 L031702, [[arXiv:2506.04568](#)].
- [33] G. Steigman, B. Dasgupta, and J. F. Beacom, *Precise Relic WIMP Abundance and its Impact on Searches for Dark Matter Annihilation*, *Phys. Rev. D* **86** (2012) 023506, [[arXiv:1204.3622](#)].
- [34] X. Chu and J. Pradler, *Minimal mass of thermal dark matter and the viability of millicharged particles affecting 21-cm cosmology*, *Phys. Rev. D* **109** (2024), no. 10 103510, [[arXiv:2310.06611](#)].
- [35] A. Granelli, S. Pascoli, and S. Rosauero-Alcaraz, *Dark Matter Interpretation of the Super-Kamiokande Antineutrino Excess and Predictions for JUNO*, [[arXiv:2605.20162](#)].
- [36] M. Endo, Y. Mura, and T. Tsuji, *Dark Matter Interpretation of the Super-Kamiokande Antineutrino Excess in $U(1)_{L_\mu-L_\tau}$ model*, [[arXiv:2605.28275](#)].
- [37] G. Mangano, G. Miele, S. Pastor, and M. Peloso, *A Precision calculation of the effective number of cosmological neutrinos*, *Phys. Lett. B* **534** (2002) 8–16, [[astro-ph/0111408](#)].
- [38] G. Mangano, G. Miele, S. Pastor, T. Pinto, O. Pisanti, and P. D. Serpico, *Relic neutrino decoupling including flavor oscillations*, *Nucl. Phys. B* **729** (2005) 221–234, [[hep-ph/0506164](#)].
- [39] P. F. de Salas and S. Pastor, *Relic neutrino decoupling with flavour oscillations revisited*, *JCAP* **07** (2016) 051, [[arXiv:1606.06986](#)].
- [40] M. Escudero, *Neutrino decoupling beyond the Standard Model: CMB constraints on the Dark Matter mass with a fast and precise N_{eff} evaluation*, *JCAP* **02** (2019) 007, [[arXiv:1812.05605](#)].
- [41] J. J. Bennett, G. Buldgen, P. F. De Salas, M. Drewes, S. Gariazzo, S. Pastor, and Y. Y. Y. Wong, *Towards a precision calculation of N_{eff} in the Standard Model II: Neutrino decoupling in the presence of flavour oscillations and finite-temperature QED*, *JCAP* **04** (2021) 073, [[arXiv:2012.02726](#)].

- [42] M. Escudero Abenza, *Precision early universe thermodynamics made simple: N_{eff} and neutrino decoupling in the Standard Model and beyond*, *JCAP* **05** (2020) 048, [[arXiv:2001.04466](#)].
- [43] M. Cielo, M. Escudero, G. Mangano, and O. Pisanti, *N_{eff} in the Standard Model at NLO is 3.043*, *Phys. Rev. D* **108** (2023), no. 12 L121301, [[arXiv:2306.05460](#)].
- [44] C. Burigana, L. Danese, and G. De Zotti, *Formation and evolution of early distortions of the microwave background spectrum - A numerical study*, *Astron. Astrophys.* **246** (1991), no. 1 49–58.
- [45] W. Hu and J. Silk, *Thermalization and spectral distortions of the cosmic background radiation*, *Phys. Rev. D* **48** (1993) 485–502.
- [46] S.-P. Li and J. Chluba, *Neutrino-genic CMB spectral distortions*, *Phys. Rev. D* **113** (2026), no. 4 043504, [[arXiv:2510.04684](#)].
- [47] R. Khatri and R. A. Sunyaev, *Beyond γ and μ : the shape of the CMB spectral distortions in the intermediate epoch, $1.5 \times 10^4 < z < 2 \times 10^5$* , *JCAP* **09** (2012) 016, [[arXiv:1207.6654](#)].
- [48] S. K. Acharya and R. Khatri, *Rich structure of non-thermal relativistic CMB spectral distortions from high energy particle cascades at redshifts $z \lesssim 2 \times 10^5$* , *Phys. Rev. D* **99** (2019), no. 4 043520, [[arXiv:1808.02897](#)].
- [49] J. Chluba and R. A. Sunyaev, *The evolution of CMB spectral distortions in the early Universe*, *Mon. Not. Roy. Astron. Soc.* **419** (2012) 1294–1314, [[arXiv:1109.6552](#)].
- [50] J. C. Mather et al., *Measurement of the Cosmic Microwave Background spectrum by the COBE FIRAS instrument*, *Astrophys. J.* **420** (1994) 439–444.
- [51] D. J. Fixsen, E. S. Cheng, J. M. Gales, J. C. Mather, R. A. Shafer, and E. L. Wright, *The Cosmic Microwave Background spectrum from the full COBE FIRAS data set*, *Astrophys. J.* **473** (1996) 576, [[astro-ph/9605054](#)].
- [52] F. Bianchini and G. Fabbian, *CMB spectral distortions revisited: A new take on μ distortions and primordial non-Gaussianities from FIRAS data*, *Phys. Rev. D* **106** (2022), no. 6 063527, [[arXiv:2206.02762](#)].
- [53] A. Sabyr, G. Fabbian, J. C. Hill, and F. Bianchini, *A new constraint on the γ -distortion with FIRAS: robustness of component separation methods*, [[arXiv:2508.04593](#)].
- [54] B. Maffei et al., *BISOU: A balloon project to measure the CMB spectral distortions*, in *16th Marcel Grossmann Meeting on Recent Developments in Theoretical and Experimental General Relativity, Astrophysics and Relativistic Field Theories*, 10, 2021. [[arXiv:2111.00246](#)].
- [55] S. Masi et al., *The cosmic monopole observer (cosmo)*, [[arXiv:2110.12254](#)].
- [56] P. Alonso-Arias et al., *A Microwave Blackbody Target for Cosmic Microwave Background Spectral Measurements in the 10-20GHz range*, [[arXiv:2309.07320](#)].
- [57] A. Sabyr, C. Sierra, J. C. Hill, and J. J. McMahon, *SPECTER: An Instrument Concept for CMB Spectral Distortion Measurements with Enhanced Sensitivity*, [[arXiv:2409.12188](#)].
- [58] A. Kogut et al., *The Primordial Inflation Explorer (PIXIE): A Nulling Polarimeter for Cosmic Microwave Background Observations*, *JCAP* **07** (2011) 025, [[arXiv:1105.2044](#)].
- [59] A. Kogut et al., *The Primordial Inflation Explorer (PIXIE): mission design and science goals*, *JCAP* **04** (2025) 020, [[arXiv:2405.20403](#)].
- [60] A. Kogut, M. H. Abitbol, J. Chluba, J. Delabrouille, D. Fixsen, J. C. Hill, S. P. Patil, and A. Rotti, *CMB Spectral Distortions: Status and Prospects*, *Bull. Am. Astron. Soc.* **51** (2019), no. 7 113, [[arXiv:1907.13195](#)].

- [61] J. Chluba et al., *New horizons in cosmology with spectral distortions of the cosmic microwave background*, *Exper. Astron.* **51** (2021), no. 3 1515–1554, [[arXiv:1909.01593](#)].
- [62] B. Batell, T. Han, D. McKeen, and B. Shams Es Haghi, *Thermal Dark Matter Through the Dirac Neutrino Portal*, *Phys. Rev. D* **97** (2018), no. 7 075016, [[arXiv:1709.07001](#)].
- [63] P. Ballett, M. Hostert, and S. Pascoli, *Dark Neutrinos and a Three Portal Connection to the Standard Model*, *Phys. Rev. D* **101** (2020), no. 11 115025, [[arXiv:1903.07589](#)].
- [64] M. Blennow, E. Fernandez-Martinez, A. Olivares-Del Campo, S. Pascoli, S. Rosauero-Alcaraz, and A. V. Titov, *Neutrino Portals to Dark Matter*, *Eur. Phys. J. C* **79** (2019), no. 7 555, [[arXiv:1903.00006](#)].
- [65] S.-P. Li and X.-J. Xu, *Dark matter produced from right-handed neutrinos*, *JCAP* **06** (2023) 047, [[arXiv:2212.09109](#)].
- [66] J. L. Feng, A. Rajaraman, and F. Takayama, *Superweakly interacting massive particles*, *Phys. Rev. Lett.* **91** (2003) 011302, [[hep-ph/0302215](#)].
- [67] J. L. Feng, A. Rajaraman, and F. Takayama, *SuperWIMP dark matter signals from the early universe*, *Phys. Rev. D* **68** (2003) 063504, [[hep-ph/0306024](#)].
- [68] T. Cohen, D. E. Morrissey, and A. Pierce, *Changes in Dark Matter Properties After Freeze-Out*, *Phys. Rev. D* **78** (2008) 111701, [[arXiv:0808.3994](#)].
- [69] M. J. Baker, J. Kopp, and A. J. Long, *Filtered Dark Matter at a First Order Phase Transition*, *Phys. Rev. Lett.* **125** (2020), no. 15 151102, [[arXiv:1912.02830](#)].
- [70] X.-R. Wong and K.-P. Xie, *Freeze-in of WIMP dark matter*, *Phys. Rev. D* **108** (2023), no. 5 055035, [[arXiv:2304.00908](#)].
- [71] **Planck** Collaboration, N. Aghanim et al., *Planck 2018 results. VI. Cosmological parameters*, *Astron. Astrophys.* **641** (2020) A6, [[arXiv:1807.06209](#)]. [Erratum: *Astron. Astrophys.* 652, C4 (2021)].
- [72] T. Hambye, M. Hufnagel, and M. Lucca, *Cosmological constraints on the decay of heavy relics into neutrinos*, *JCAP* **05** (2022), no. 05 033, [[arXiv:2112.09137](#)].
- [73] S.-P. Li and X.-J. Xu, *N_{eff} constraints on light mediators coupled to neutrinos: the dilution-resistant effect*, *JHEP* **10** (2023) 012, [[arXiv:2307.13967](#)].
- [74] S. Bianco, P. F. Depta, J. Frerick, T. Hambye, M. Hufnagel, and K. Schmidt-Hoberg, *Photo- and Hadrodisintegration constraints on massive relics decaying into neutrinos*, [[arXiv:2505.01492](#)].
- [75] S. Chang, S. Ganguly, T. H. Jung, T.-S. Park, and C. S. Shin, *Constraining MeV to 10 GeV Majorons by big bang nucleosynthesis*, *Phys. Rev. D* **110** (2024), no. 1 015019, [[arXiv:2401.00687](#)].
- [76] J. A. Formaggio and G. P. Zeller, *From eV to EeV: Neutrino Cross Sections Across Energy Scales*, *Rev. Mod. Phys.* **84** (2012) 1307–1341, [[arXiv:1305.7513](#)].
- [77] S. Borsanyi et al., *Calculation of the axion mass based on high-temperature lattice quantum chromodynamics*, *Nature* **539** (2016), no. 7627 69–71, [[arXiv:1606.07494](#)].
- [78] M. Kawasaki and T. Moroi, *Gravitino decay into a neutrino and a sneutrino in the inflationary universe*, *Phys. Lett. B* **346** (1995) 27–34, [[hep-ph/9408321](#)].
- [79] S. K. Acharya and R. Khatri, *Constraints on N_{eff} of high energy non-thermal neutrino injections upto $z \sim 10^8$ from CMB spectral distortions and abundance of light elements*, *JCAP* **11** (2020) 011, [[arXiv:2007.06596](#)].

- [80] T. Kanzaki, M. Kawasaki, K. Kohri, and T. Moroi, *Cosmological Constraints on Neutrino Injection*, *Phys. Rev. D* **76** (2007) 105017, [[arXiv:0705.1200](#)].
- [81] J. Gratsias, R. J. Scherrer, and D. N. Spergel, *Indirect photofission of light elements from high-energy neutrinos in the early universe*, *Phys. Lett. B* **262** (1991) 298–302.
- [82] A. A. de Laix and R. J. Scherrer, *Improved cosmological constraints on neutrino producing decaying particles*, *Phys. Rev. D* **48** (1993) 562–566.
- [83] P. McDonald, R. J. Scherrer, and T. P. Walker, *Cosmic microwave background constraint on residual annihilations of relic particles*, *Phys. Rev. D* **63** (2001) 023001, [[astro-ph/0008134](#)].
- [84] G. R. Blumenthal and R. J. Gould, *Bremsstrahlung, synchrotron radiation, and compton scattering of high-energy electrons traversing dilute gases*, *Rev. Mod. Phys.* **42** (1970) 237–270.
- [85] X.-L. Chen and M. Kamionkowski, *Particle decays during the cosmic dark ages*, *Phys. Rev. D* **70** (2004) 043502, [[astro-ph/0310473](#)].
- [86] N. Padmanabhan and D. P. Finkbeiner, *Detecting dark matter annihilation with CMB polarization: Signatures and experimental prospects*, *Phys. Rev. D* **72** (2005) 023508, [[astro-ph/0503486](#)].
- [87] S. Hannestad, *Oscillation effects on neutrino decoupling in the early universe*, *Phys. Rev. D* **65** (2002) 083006, [[astro-ph/0111423](#)].
- [88] A. D. Dolgov, S. H. Hansen, S. Pastor, S. T. Petcov, G. G. Raffelt, and D. V. Semikoz, *Cosmological bounds on neutrino degeneracy improved by flavor oscillations*, *Nucl. Phys. B* **632** (2002) 363–382, [[hep-ph/0201287](#)].
- [89] S.-P. Li, *Observability of CMB spectrum distortions from dark matter annihilation*, *JCAP* **07** (2024) 019, [[arXiv:2402.16708](#)].
- [90] R. A. Sunyaev and Y. B. Zeldovich, *The Interaction of matter and radiation in the hot model of the universe*, *Astrophys. Space Sci.* **7** (1970) 20–30.
- [91] R. Khatri and R. A. Sunyaev, *Creation of the CMB spectrum: precise analytic solutions for the blackbody photosphere*, *JCAP* **06** (2012) 038, [[arXiv:1203.2601](#)].
- [92] J. Chluba, *Refined approximations for the distortion visibility function and μ -type spectral distortions*, *Mon. Not. Roy. Astron. Soc.* **440** (2014), no. 3 2544–2563, [[arXiv:1312.6030](#)].
- [93] J. Chluba, *Which spectral distortions does Λ CDM actually predict?*, *Mon. Not. Roy. Astron. Soc.* **460** (2016), no. 1 227–239, [[arXiv:1603.02496](#)].
- [94] S. Horiuchi, J. F. Beacom, and E. Dwek, *The Diffuse Supernova Neutrino Background is detectable in Super-Kamiokande*, *Phys. Rev. D* **79** (2009) 083013, [[arXiv:0812.3157](#)].
- [95] N. F. Bell, M. J. Dolan, and S. Robles, *Searching for Sub-GeV Dark Matter in the Galactic Centre using Hyper-Kamiokande*, *JCAP* **09** (2020) 019, [[arXiv:2005.01950](#)].
- [96] M. Honda, M. Sajjad Athar, T. Kajita, K. Kasahara, and S. Midorikawa, *Atmospheric neutrino flux calculation using the NRLMSISE-00 atmospheric model*, *Phys. Rev. D* **92** (2015), no. 2 023004, [[arXiv:1502.03916](#)].
- [97] **Simons Observatory** Collaboration, P. Ade et al., *The Simons Observatory: Science goals and forecasts*, *JCAP* **02** (2019) 056, [[arXiv:1808.07445](#)].
- [98] **Simons Observatory** Collaboration, M. H. Abitbol et al., *The Simons Observatory: Astro2020 Decadal Project Whitepaper*, *Bull. Am. Astron. Soc.* **51** (2019) 147, [[arXiv:1907.08284](#)].

- [99] **Super-Kamiokande** Collaboration, H. Zhang et al., *Supernova Relic Neutrino Search with Neutron Tagging at Super-Kamiokande-IV*, *Astropart. Phys.* **60** (2015) 41–46, [[arXiv:1311.3738](#)].
- [100] K. M. Nollett and G. Steigman, *BBN And The CMB Constrain Neutrino Coupled Light WIMPs*, *Phys. Rev. D* **91** (2015), no. 8 083505, [[arXiv:1411.6005](#)].
- [101] N. Sabti, J. Alvey, M. Escudero, M. Fairbairn, and D. Blas, *Addendum: Refined bounds on MeV-scale thermal dark sectors from BBN and the CMB*, *JCAP* **08** (2021) A01, [[arXiv:2107.11232](#)].
- [102] X. Chu, J.-L. Kuo, and J. Pradler, *Toward a full description of MeV dark matter decoupling: A self-consistent determination of relic abundance and N_{eff}* , *Phys. Rev. D* **106** (2022), no. 5 055022, [[arXiv:2205.05714](#)].
- [103] **DESI** Collaboration, A. G. Adame et al., *DESI 2024 VI: cosmological constraints from the measurements of baryon acoustic oscillations*, *JCAP* **02** (2025) 021, [[arXiv:2404.03002](#)].
- [104] **DESI** Collaboration, W. Elbers et al., *Constraints on Neutrino Physics from DESI DR2 BAO and DR1 Full Shape*, [arXiv:2503.14744](#).
- [105] **SPT-3G** Collaboration, F. Ge et al., *Cosmology From CMB Lensing and Delensed EE Power Spectra Using 2019-2020 SPT-3G Polarization Data*, [arXiv:2411.06000](#).
- [106] **ACT** Collaboration, E. Calabrese et al., *The Atacama Cosmology Telescope: DR6 Constraints on Extended Cosmological Models*, [arXiv:2503.14454](#).